Insights into flow and heat transfer aspects of hypersonic rarefied flow over a blunt body with aerospike using direct simulation Monte-Carlo approach

Arun Kumar Chinnappan [1], Malaikannan G. [1], Rakesh Kumar *,[2]

Indian Institute of Technology Kanpur, Uttar Pradesh, 208016, India

A B S T R A C T

Hypersonic aero-thermodynamic study of a blunt body with different aerospike configurations is carried out in the Direct Simulation Monte Carlo framework. Influence of aerospike geometry variation on the surface properties such as drag coefficient and convective heat transfer rate are analyzed for a freestream Mach number of 5.75 at 70 km altitude. Numerical investigations are done by varying the diameter of an aerodisk/front body and aerospike length. The simulation results show that an aerodisk of appropriate length and diameter reduces drag coefficient significantly with a moderate value of heat flux. The aerospike length significantly changes the flow behavior and results in some interesting flow features that alter drag and heat flux variation on the surface.

1. Introduction

A main challenge in the design of hypersonic vehicles is to reduce aerodynamic heating and drag. The blunt body configuration is currently in use to reduce aerodynamic heating to the surface but it leads to significant increase in the drag. Although blunt body design works well for planetary re-entry vehicles, which require a large value of drag with reduced aerodynamic heating, it is unfavorable for other hypersonic vehicle applications such as launch vehicles and missiles. The increase in drag value affects the overall performance of such hypersonic vehicles, such as decreased speed range, increased fuel consumption rate and reduced payload carrying capacity. The slender bodies are effective in controlling the oblique shocks and their impingement locations, but suffer from severe aerodynamic heating. Thus, an effective design is a trade-off between slender and blunt bodies. The nose of a vehicle is of principal interest and numerous methods have been considered for an improvised design of a hypersonic vehicle with respect to the aforesaid parameters. Some of these techniques include the use of concentrated energy deposition along the stagnation streamline [1], aerospike ahead of the blunt body [2], forward facing jet in the stagnation zone of the blunt body [3], counter flow drag reduction technique [4] and the use of supersonic projectiles fired in the upstream direction from the stagnation zone [5].

Among those techniques, the use of aerospike ahead of the blunt body was found to be simple and most efficient way in reducing drag and aerodynamic heating. Crawford [6] studied the hypersonic flow over a spiked-nose hemispherical cylinder and found that drag was reduced with an increase in spike length. Several experimental and numerical studies have been done on reducing drag on hypersonic flows [7–11]. The inspiration for this study is obtained from the experimental work carried out by Menezes [2] together with numerical studies conducted using the commercial software CFX. In this work, a forebody with a spike is introduced upstream of the main body. The experiment is conducted at a freestream Mach number of 5.75 while varying the forebody geometry and spike length. The effect of the variations on the drag coefficient and heat transfer are studied. However, a significant discrepancy between the experimental and numerical results was observed for drag coefficient and surface heat flux, which is not surprising considering the limitations associated with the Navier-Stokes based methods for modeling high Mach number flow, particularly at high altitudes.

Since the present study includes highly non-equilibrium regions such as shock–shock and shock–wave boundary layer interactions, the theoretical study of the same becomes extremely complex, whereas the use of a continuum solver becomes questionable. Therefore, we have used a kinetic particle based method, such as the Direct Simulation Monte-Carlo (DSMC) method, for an accurate study of hypersonic semi-rarefied gas flow over a blunt body

* Corresponding author.
  E-mail address: rkm@iitk.ac.in (R. Kumar).
[1] Research Scholar, Department of Aerospace Engineering.
[2] Assistant Professor, Department of Aerospace Engineering.

Nomenclature

|			
M_∞	Mach number	$\bar{c}$	Average thermal speed
d	Diameter of the aerodisk	C_h	Stanton number
D	Diameter of the main body	ρ_∞	Freestream density
L	Spike length	v_∞	Freestream velocity
C_d	Coefficient of drag	C_p	Coefficient of pressure
Q_{max}	Peak heat flux	T_{aw}	Adiabatic wall temperature
λ	Mean free path	T_{body}	Body temperature
n_∞	Freestream number density	$Q(t)$	Heat flux
τ	Mean collision time		
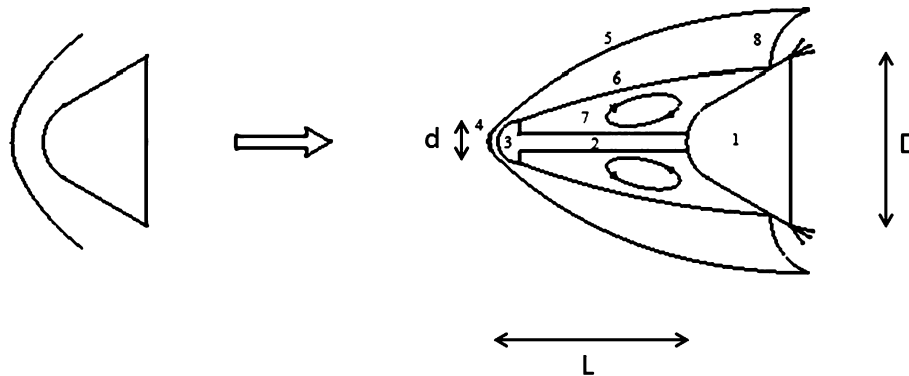
Fig. 1. Flow features around the blunt cone without spike and with spike.

(representing nose of a high speed vehicle) with different kinds of aerospike configurations. The main aim of this study is to propose a design that could result in a lower surface heat flux and a reasonably low drag coefficient. In the first stage of the current study, the diameter ratio is varied, whereas in the second stage, the spike length is varied for fixed fore and main body geometries. The effect of shock reattachment location, size of the recirculation region on the drag coefficients are also studied.

The remainder of the paper is presented as follows. In Sec. 2, the concept of aerospike is briefly introduced. Section 3 explains the computational model used in this study. Section 4 presents two validation studies of the in-house DSMC solver, named as Non-equilibrium Flow Solver (NFS), with published DSMC results. The numerical parameters for the present problem of hypersonic flow over a blunt body with aerospike are presented in Section 6. This is followed by the discussion of results in Sec. 7. Finally the conclusions are presented in Sec. 8.

2. Concept of aerospike

When a blunt body is subjected to hypersonic flow, it creates a strong bow shock with a large increase in temperature, which heats the air rather than the surface of the body. The primary aim of introducing aerospike is to reduce drag by replacing the strong bow shock into weaker oblique shocks without much increase in heat flux. The flow separates at the front body (aerodisk) due to adverse pressure gradient and reattaches at the main body, creating a large recirculation region as shown in Fig. 1. The streamline separating the streamlines, which are moving downstream and trapped inside the dead air region (recirculation region) is called dividing streamline [12], the term was first introduced by Chapman et al. [13]. The numbers in the Fig. 1 denotes: 1. Blunt/main body; 2. Spike; 3. Front body/aerodisk; 4. Disk bow shock; 5. Shock due to flow separation; 6. Shear layer; 7. Recirculation region; 8. Re-attachment shock.

3. The DSMC method

DSMC was first proposed by G.A. Bird for rarefied flows [14]. This method deals with simulated molecules, each of which represents a large number of real molecules. The primary assumption in DSMC is the decoupling of molecular movement and intermolecular collisions (considered instantaneous), due to this decoupling, the time step used in DSMC is typically kept less than the mean collision time and the cell size should be less than the mean free path of the gas. The DSMC method involves discretization of the computational domain into cells and sorting of the molecules by their position coordinates. Molecules are moved in a deterministic way followed by their collisions in a probabilistic manner using the acceptance-rejection method. In the present work, an in-house 2D parallel multi-species DSMC solver, named as Non-equilibrium Flow Solver (NFS), is developed and used [15,16]. Some specific features of the solver are as follows: The post collision velocities are determined using the Variable Hard Sphere (VHS) model. The continuous Larsen–Borgnakke (LB) model [17] is used to model rotational mode and the quantum version of LB model is applied to the vibrational modes. Bird's [14] no-time-counter model is used to calculate number of collisions. Maxwell [18] and Cercignani Lampis and Lord (CLL) model [19] are used for gas-surface interactions. The macroscopic parameters are calculated by time averaging the sampled data. The cells are adapted based on local Knudsen number to capture large flow gradients and to improve computational accuracy [20].

4. Solver validation

A recently developed two-dimensional, multispecies, parallel in-house DSMC solver, NFS, is used in this study [15]. The present solver is validated with the published DSMC results [21,22], before applying it to the aerospike problem, which is the subject of the present work. The flow properties are compared in the first validation case-study, whereas the second validation case-study presents

Table 1
Free stream conditions for first validation case: wedge.

Velocity (m/s)	5500
Temperature (K)	1100
Density (kg/m³)	0.0026
Knudsen number	6.54×10^{-4}
Mole fraction	$N_2 : 0.806, N : 0.194$
Mach number	7.7
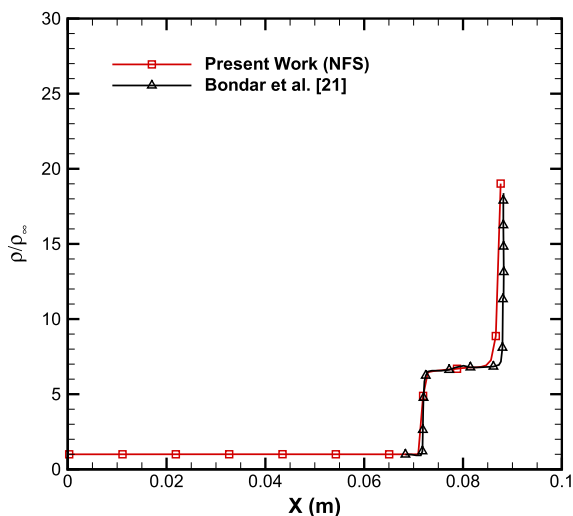
Fig. 2. Density comparison along the stagnation streamline.

Fig. 3. Temperature comparison along the stagnation streamline.

Table 2
Free stream conditions for second validation case: 2D cylinder.

Velocity (m/s)	2624.1
Temperature (K)	198
Number density (1/m³)	1.699×10^{19}
Knudsen number	0.25
Mach number	10

Fig. 4. Comparision of heat flux with Lofthouse et al.

comparision of surface properties. Diffuse reflection is assumed for both of the case studies. Variable Hard Sphere (VHS) model is used to calculate post-collision velocities, along with LB model for energy exchange between internal modes. In both of the validation case-studies, the time step and cell size were kept respectively less than the mean collision time and mean free path corresponding to the free stream conditions. The statistical error is found to be less than 2%.
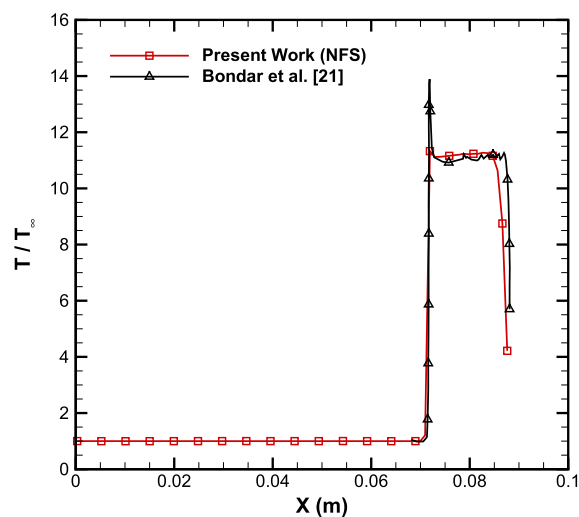
4.1. Flow over a 2D wedge at Mach 7.7

The first validation case-study encompasses Mach 7.7 flow over a wedge at near-continuum regime. The wedge is at an angle of 62.5° and length of 0.051 m. The freestream conditions are taken from Bondar et al. [21] and are given in Table 1. The CLL model with fully diffuse wall condition, which corresponds to an accommodation coefficient of 1, is used to model gas-surface interactions.

Figs. 2 and 3 show the density and translational temperature variation along the stagnation streamline. Both, translational temperature and density are normalized with the respective freestream values. It is observed that the flow properties are in good agreement with those obtained by Bondar et al. [21]. Moreover, it is evident from the Figs. 2, 3 that the shock standoff distance also agrees well with that predicted by Bondar et al. [21]

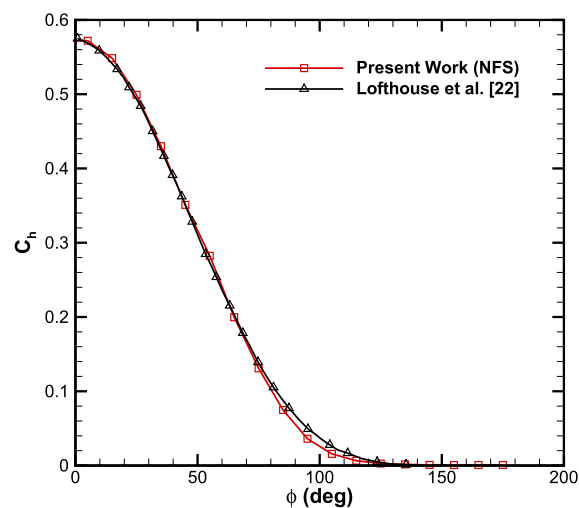### 4.2. Argon flow over a 2D cylinder at Mach 10

The second validation case study involves a hypersonic Mach 10 argon flow over a 2D cylinder (diameter = 0.3048 m) at two different Knudsen numbers. The input parameters for Knudsen number of 0.25 case, are taken from Lofthouse et al. [22] and given in Table 2. The CLL gas-surface interaction model is used with an accommodation coefficient of unity.

Table 3 compares the total drag and peak heat transfer rates predicted by the present DSMC solver with those obtained by Lofthouse et al. [22] at different Knudsen numbers. The pressure drag

force is computed by sampling the normal momentum change, while the skin friction drag is calculated by sampling the tangential momentum change. The total drag presented in Table 3 is the sum of skin friction and pressure drag. The heat flux is evaluated by sampling the difference in energy of the particles before and after hitting the surface. The values obtained from the present solver are in good agreement with those obtained by Lofthouse et al. [22]. The maximum error is found to be less than 4%. Moreover, the normalized heat transfer coefficient C_h along the cylinder surface agrees fairly well with that predicted by Lofthouse et al. [22]. (Fig. 4)

5. Grid sensitivity study

The grid sensitivity study has been done for the present problem of flow over a blunt body with aerospike. To this end, we

Table 3
Comparison of drag and peak heat transfer rate.

Knudsen number	Lofthouse et al. [22]		Present Results	
	Q_{max} kW/m^2	Drag/Length (N/m)	Q_{max} kW/m^2	Drag/Length (N/m)
0.05	15.92	8.9	16.072	8.72
0.25	5.926	2.092	5.825	2.17

(a) without adaptation (250000 cells)

(b) 1st adaptation level (346979 cells)

(c) 2nd adaptation level (570000 cells)

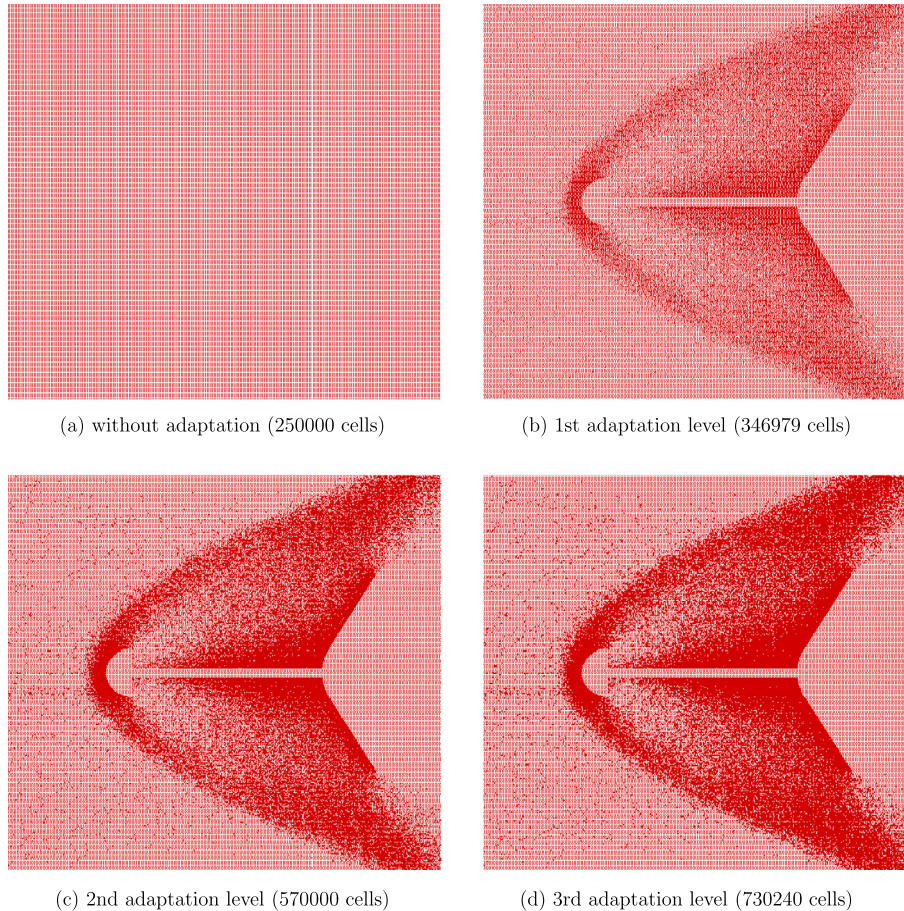(d) 3rd adaptation level (730240 cells)

Fig. 5. Comparison of grid for different adaptation levels.

have carried out a case study, the parameters for which are obtained from the experimental investigations of Menezes et al. [2]. The model used in their work is a bicone with aerodisk at the front. The freestream Mach and Reynolds numbers are $M_\infty = 5.75$ and $Re_\infty = 1.5 \times 10^6$, respectively. The problem has been simulated in the DSMC framework, wherein the cell size and time step are ideally to be kept less than the mean free path and mean collision time, respectively. However, because of high number density near shock region, the actual cell size may be greater than the local mean free path, which violates the primary requirement of the DSMC method. Therefore, the cells are adapted in those regions, wherever the local cell size is higher than the local mean free path. Figures for different adaptation levels are shown in Fig. 5. The non-equilibrium regions such as shock and boundary layer regions are adapted, so that it can capture more number of collisions and improve the accuracy. The total drag coefficient for different levels of adaptations is shown in Table 4.

As evident from the table, the drag coefficient value obtained in this work agrees very well with the value reported in experiments [2]. The total drag obtained from the third level of adaptation agrees well with the experimental result. Moreover, the drag

value predicted from the third and fourth level of adaptations are almost the same, and differ from experiments is less than 0.5%. Therefore, we have used three levels of adaptation for our main studies, presented below.

6. Numerical parameters

Freestream conditions corresponding to an altitude of 70 km are chosen for this study. The choice of this altitude is governed by the fact that the DSMC method gets computationally very expensive to simulate flow at low altitudes or high number densities. The freestream Mach number at this altitude is taken as 5.75, which is the value chosen in experimental work of Menezes et al. [2]. The freestream Knudsen number, temperature, pressure and density are 7.2×10^{-3}, 219.5 K, 5.2209 Pa and $8.2829 \times 10^{-5} \frac{kg}{m^3}$ respectively. Nitrogen is used as a gas with the consideration of high temperature effects, such as vibrational excitation. The post collision velocities are determined using the Variable Hard Sphere (VHS) model. The chemical reactions such as dissociation and recombination are not considered in the present study, as the stagnation temperature, 1670.94 K, is comparatively low for reactions
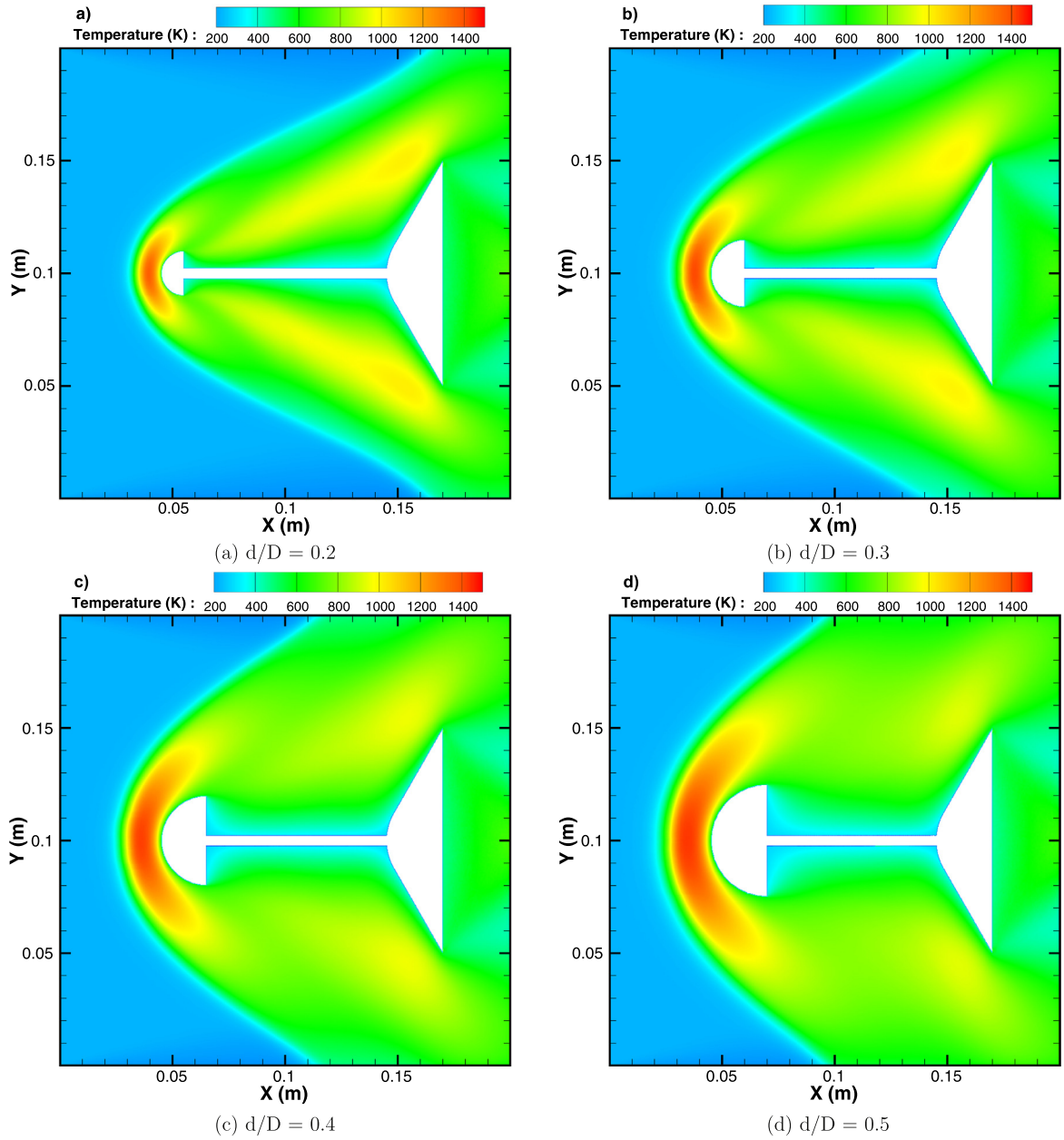
(a) d/D = 0.2

(b) d/D = 0.3

(c) d/D = 0.4

(d) d/D = 0.5

Fig. 6. Temperature contours for different d/D ratios at fixed L/D = 1.

Table 4
Variation of drag coefficient with adaptation levels.

Adaptation level	No. of cells	DSMC result (C_d)	Exp. value (C_d) [2]
0	250000	0.64190	0.757
1	346979	0.67300	0.757
2	570000	0.69310	0.757
3	730240	0.75806	0.757
4	840040	0.76140	0.757
5	854320	0.76172	0.757

to take place. The body is considered to be at 288 K temperature, while diffuse boundary condition with accommodation coefficient (both normal and tangential) of 1 is assumed on the surface using the CLL model. The time step was chosen to be 9×10^{-7} s, which is smaller than the mean collision time (1.8×10^{-6} s). The initial number of cells was 640000 such that the cell size 2.5×10^{-4} m less than the mean free path 7.3×10^{-4} m and adaptation was done based on the local Knudsen number to resolve shock re-

gions. The equations for mean free path and mean collision time are given below:

Mean free path, λ, given by the hard sphere model, is given by,

$$\lambda = \frac{1}{\sqrt{2}\pi d^2 n_\infty} \tag{1}$$

where, d is diameter of the molecule, n_∞ is freestream number density.

Mean collision time, τ, is given by,

$$\tau = \lambda/\bar{c} \tag{2}$$

where, $\bar{c}$ is average thermal speed.

Approximately 1.8 million simulated particles are used in this present simulation. The calculations have been performed using 20 Intel Xeon E5-2670 processors with a computational time of $\sim$100 CPU hours. The statistical error associated with these calculations is $\sim$3%.
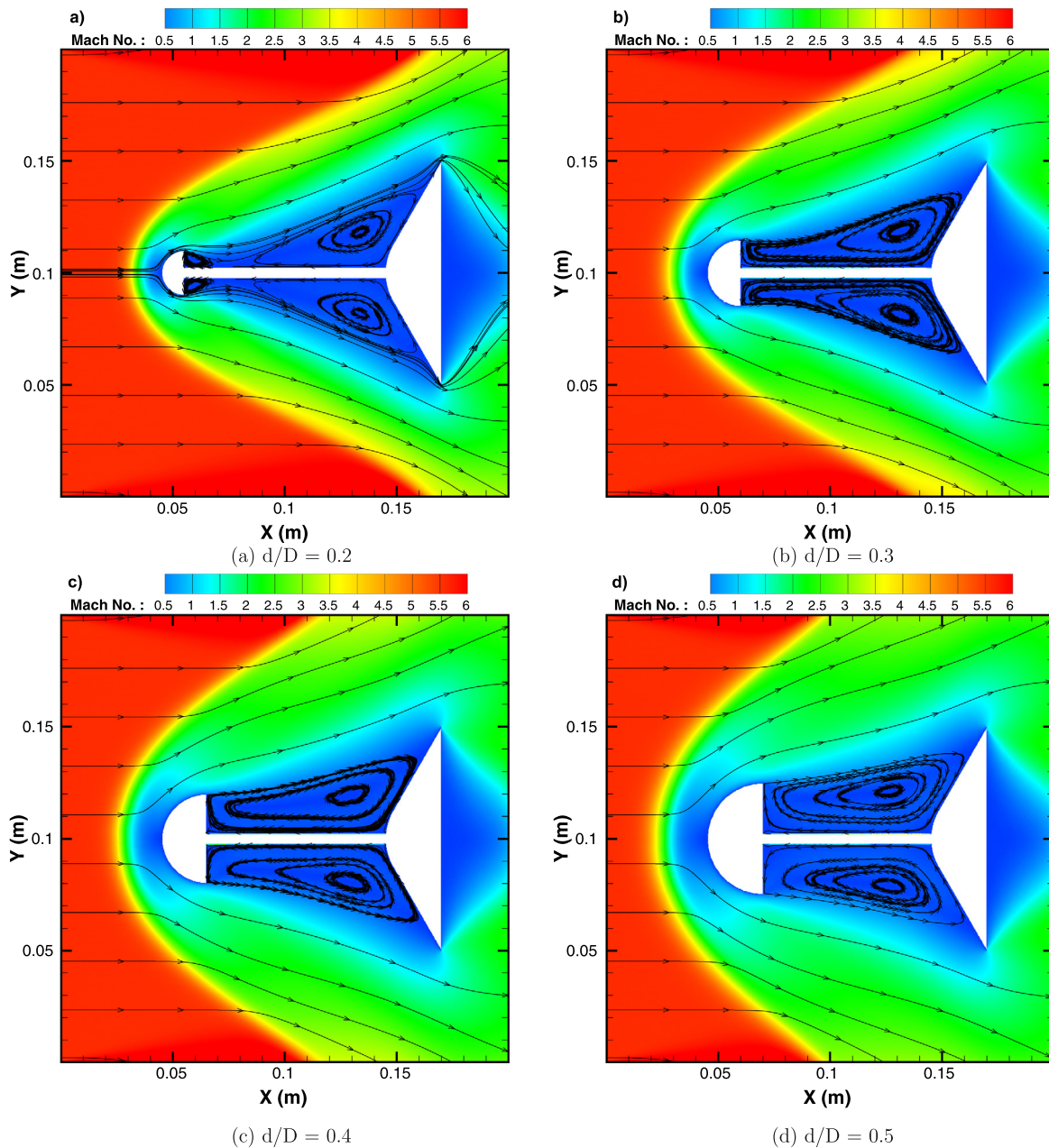
(a) d/D = 0.2

(b) d/D = 0.3

(c) d/D = 0.4

(d) d/D = 0.5

Fig. 7. Mach number contours for different d/D ratios at fixed L/D = 1.

7. Results and discussion

7.1. Flow properties

The overall temperature (weighted average of translational, rotational and vibrational) and Mach number contour for L/D = 1 and different d/D are shown in Figs. 6 and 7 respectively. Here, 'd' refers to the diameter of the aerodisk, 'D' refers to the diameter of the blunt (main) body, whereas 'L' is the length of the aerospike, as shown in Fig. 1. For d/D = 0.1, flow is separated after passing the aerodisk, it reattaches with the aerospike surface and flow becomes parallel to the aerospike (boundary layer is attached). The tip of the aerodisk creates an expansion wave to turn the flow outside the shear layer in the direction parallel to it. This shear layer, then separates and forms a recirculation region, which acts as an effective body, such that the flow outside the shear layer is parallel to it. The separated shear layer acts as a compression ramp for the upstream flow so that it produces "separation shock". The area of

recirculation region is large and it ends almost at 75% of the cone height so that the blunt body acts as a compression ramp for the incoming supersonic flow and creates a weak shock called the "Reattachment shock" near the tip. Then, expansion waves are formed at the tip of the main body, which further weaken the reattachment shock.

As d/D ratio increases, the separation point moves upstream and further away from the body axis, which increases the area of recirculation region. Therefore, the location of separation shock also moves upstream and the location of reattachment shock moves downstream. As the d/D ratio approaches its largest chosen value of 0.5, the area of recirculation zone is larger, which reduces heat transfer to the main body, but the bow shock produced by aerodisk becomes stronger and there is a large increase in temperature at the aerodisk.

Fig. 8 shows overall temperature and Mach number variation along the stagnation streamline for different d/D cases. The shock becomes more detached from the body as aerodisk diameter in-
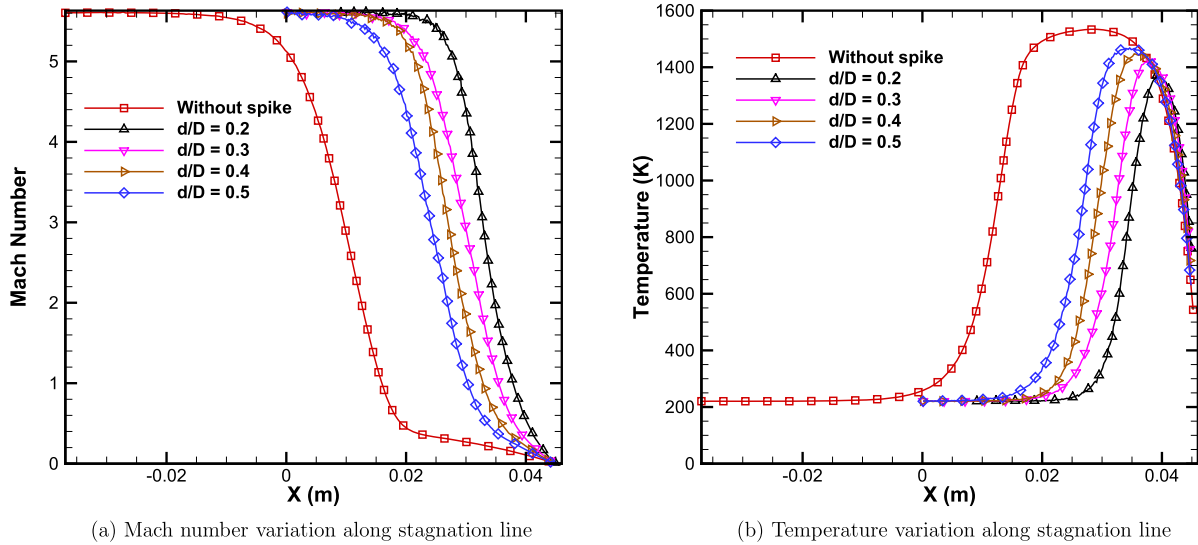
(a) Mach number variation along stagnation line

(b) Temperature variation along stagnation line

Fig. 8. Comparison of flow properties along the stagnation streamline for different d/D cases.
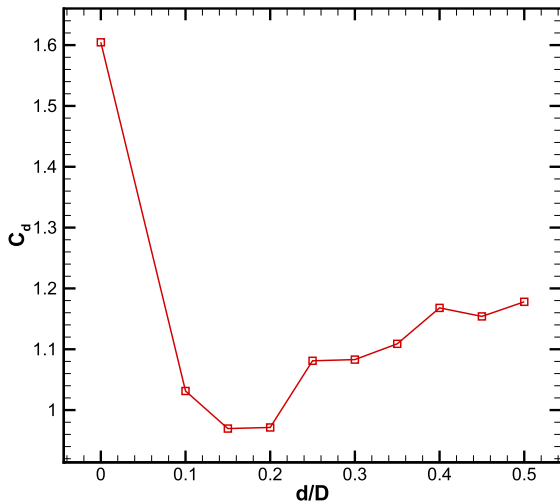

Fig. 9. Comparison of drag coefficient for different d/D ratios at fixed L/D = 1.

creases. The temperature profile shows that the shock strength (as indicated by difference in temperatures before and after the shock) increases with increasing aerodisk diameter. Results obtained for body without aerospike are also plotted in the figure to show that the shock strength and stand-off distance are reduced significantly due to aerospike. The largest shock stand-off distance of 0.037 m is observed for body without spike case. The d/D ratio of 0.2 contributes smallest shock stand-off distance of 0.0124 m, which is almost 33% of the largest value.

7.2. Drag comparison

The drag comparison for different d/D ratios is illustrated in Fig. 9. A sudden drop in drag coefficient is observed from no-spike case to d/D ratio of 0.1, which corresponds to body with spike but no aerodisk at the front. The drag coefficient decreases as d/D increases from a value of 0.1 to 0.2, after which it increases again. It is observed that the drag coefficient is almost equal for both d/D = 0.15 and 0.2. The shock at the front body is weaker for low d/D ratios and it gets stronger when d/D increases, so the effective body becomes more blunt, which causes the drag coefficient to increase with an increase in d/D after 0.2. Therefore, the separated bound-

ary layer from the aerodisk merges with the recirculation region for a d/D value more than 0.2. Also, from our study, we have observed that aerospike with small aerodisk (d/D ≤ 0.2) results in a smaller drag value than spike without aerodisk.

7.3. Heat flux comparison

Besides the drag, another important parameter for a high speed vehicle is the surface heat flux. The effect of aerospike on the same is discussed as follows. The heat flux is non-dimensionalized in the form of Stanton number C_h based on the freestream conditions, given by the expression:

$$C_h = \frac{Q(t)}{\rho_\infty v_\infty C_p (T_{aw} - T_{body})} \tag{3}$$

The comparison of normalized heat flux values, C_h, along the length of aerospike for different d/D ratios is illustrated in Fig. 10. In all the cases, maximum heat flux is observed at the stagnation point. The d/D value of 0.5 gives smaller heat flux than all other d/D values. This is due to the presence of strongest bow shock in front of the aerodisk for d/D value of 0.5, which results in heating of air in the shock layer than surface. It is also observed that spike without aerodisk produces high heat flux, which again proves that spike with aerodisk works better than without aerodisk. It is clear from the figure that the low d/D ratios give more heat flux, which is not efficient for high speed vehicle design. On the other hand, the large d/D ratios give low heat flux values, but affected by large drag coefficients, as discussed in Sec. 7.2.

The comparison of heat flux along the main body surface for different d/D ratios is illustrated in Fig. 11. Noteworthy is the fact that heat flux profile is also given when there is no spike on the main body. Thus, the figure compares the heat flux values with and without spike. The total temperature variation near the main body shown in Fig. 12, explains the reason behind heat flux reduction along the main body. Due to the formation of recirculation region ahead of the main body, the total temperature near the main body is very low as compared to the free stream total temperature, which results in lower heat flux value. Therefore, as the aerodisk diameter increases, the total temperature near the main body decreases due to large recirculation region, which results in decreasing heat flux as shown in Fig. 11. The other interesting feature in Fig. 11 is the absence of peak heat flux at the stagnation point of the main body. On the contrary, minimum heat flux is
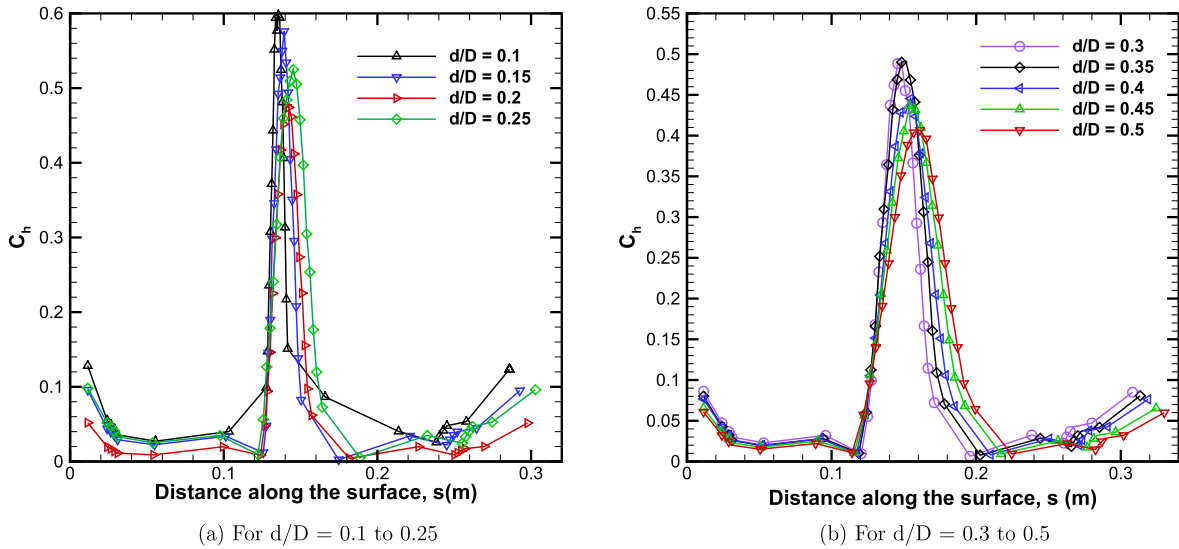
(a) For d/D = 0.1 to 0.25

(b) For d/D = 0.3 to 0.5

Fig. 10. Comparison of heat flux for different d/D ratios.

(a) For d/D = 0.1 to 0.25
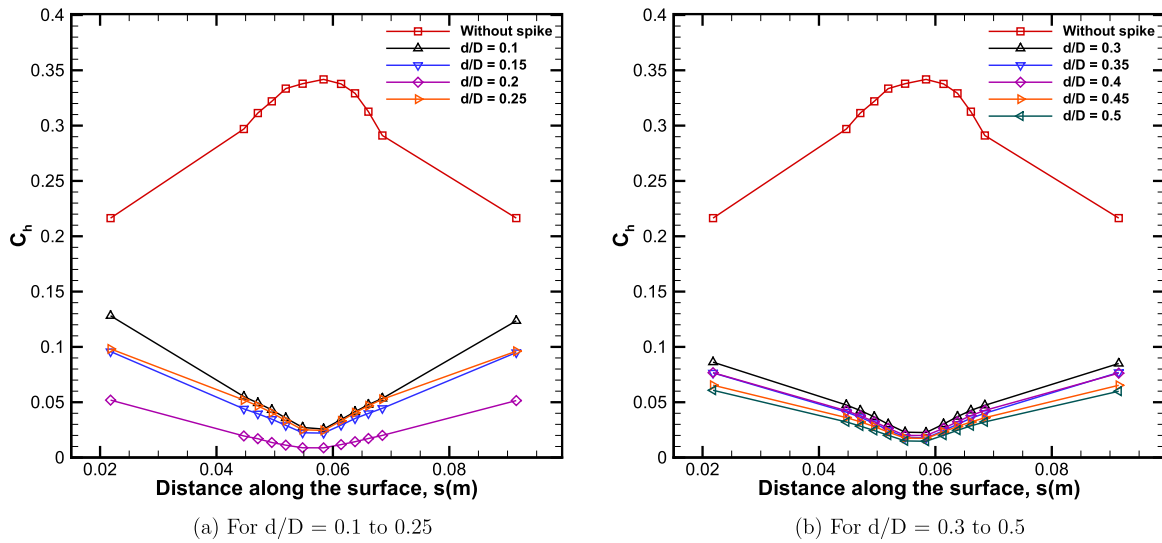
(b) For d/D = 0.3 to 0.5

Fig. 11. Comparison of heat flux along the main body for different d/D ratios.

observed at the main body stagnation point. To find the effective design, we have calculated the percentage decrease in drag coefficient and percentage increase in maximum Stanton number (at the aerodisk stagnation point) for different d/D ratios and shown in Table 5.

It is observed that low d/D ratios reduce C_d sufficiently with more than 60% increase in $(C_h)_{max}$, which is not effective for high speed vehicle design. It is found that the d/D value of 0.2 performs better than all other cases, because it gives 40% drag reduction with 35% increase in maximum heat flux. These results are derived from analyses carried out at a fixed aerospike length at L/D value of 1. In the following Section, we have carried out sensitivity study with respect to aerospike length at a fixed value of aerodisk diameter.

7.4. L/D variation

The variation of drag coefficient, C_d, and normalized heat flux, C_h, for different L/D ratios with fixed d/D of 0.2 and 0.3 is illustrated in Fig. 13. The d/D = 0.3 case predicts less drag coefficient than 0.2 for all cases except for L/D = 1. In both cases, the drag
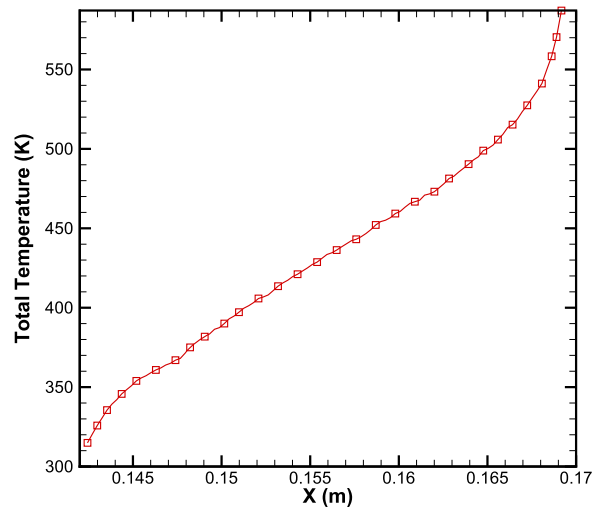

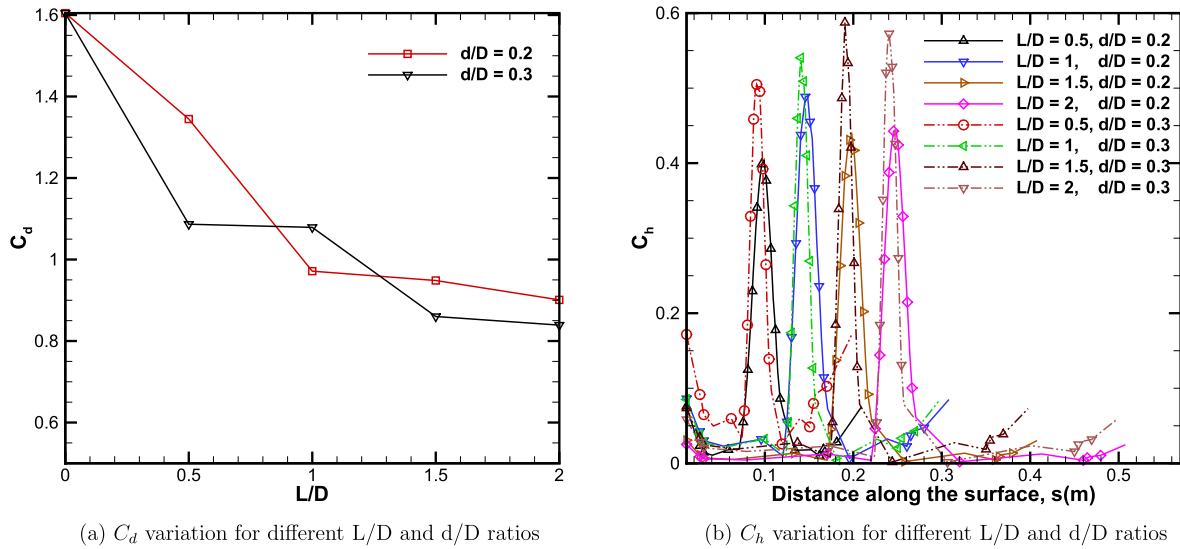**Fig. 12.** Total temperature variation along the line close to the main body.

(a) C_d variation for different L/D and d/D ratios

(b) C_h variation for different L/D and d/D ratios

Fig. 13. Comparison of C_d and C_h for different L/D ratios with fixed d/D = 0.2 and d/D = 0.3.

(a) For d/D = 0.2

(b) For d/D = 0.3

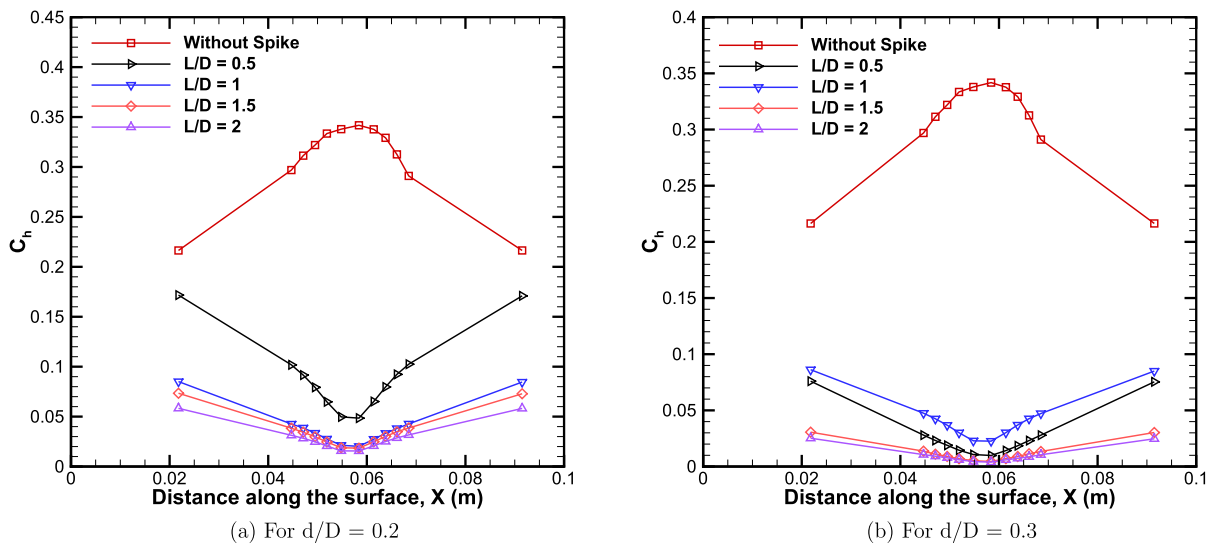**Fig. 14.** Comparison of heat flux along the main body for different L/D ratios for (a) d/D = 0.2 and (b) d/D = 0.3.

coefficient decreases with increase in aerospike length. As spike length increases, the separated boundary layer reattaches with the spike surface, and does not merge with the recirculation region ahead of the main body. This phenomenon makes the body slender effectively. This is the reason for decrease in C_d with an increase in L/D ratio.

The effect of L/D ratio on heat flux is discussed next. As L/D increases, the body becomes slender effectively and this leads to an increase in heat flux as shown in Fig. 13. The comparison of normalized heat flux along the main body is shown in Fig. 14. It is observed that, heat flux along the main body decreases as L/D decreases. However, it is observed that for a d/D value of 0.3, the heat flux for L/D = 0.5 is found to be lower than that for L/D = 1. This is because at a higher d/D (0.3) ratio and smaller L/D (0.5) ratio, the effective body formed by the shear layer is more blunt, which reduces heat flux. The other interesting observation is that the L/D ratio of 0.5 gives a good trade-off between drag and heat flux than L/D ratio of 1.0 for a d/D value of 0.3. Therefore, the effective aerospike design depends not only on aerodisk diameter but also on aerospike length.

Table 5
Comparison of % decrease in C_d and % increase in $(C_h)_{max}$ with different d/D ratios.

d/D ratio	% decrease in C_d	% increase in $(C_h)_{max}$
0.10	35.72	70.81
0.15	39.50	67.19
0.20	39.40	34.69
0.25	32.60	53.21
0.30	32.50	42.95
0.35	30.89	43.67
0.40	27.20	29.82
0.45	28.08	27.69
0.50	26.59	19.01

8. Conclusions

The hypersonic flow over a blunt body with aerospike was studied for the varying forebody diameter and length of the spike. By introducing the spike ahead of the blunt body, the high drag force produced by hypersonic vehicle is reduced significantly due to the formation of recirculation region, which makes the effective body slender. The total temperature at the recirculation region is quite

low, which resulted in reduced heat flux. The changes in flow features were explained using temperature and Mach number contour plots. The surface properties such as drag and heat flux were also compared for various configurations. It was found that large length and small forebody diameter produce less drag but high heat flux. Also, higher forebody diameter resulted in less heat flux and high drag coefficient. The forebody with diameter of 25% of main body diameter produced a lower heat flux with moderate drag coefficient. The present study was done at 70 km altitude at fixed Mach number of 5.75, but the flow behavior may change at lower altitudes and different Mach numbers. Further studies need to be done with varying forebody shape at different altitudes and Mach numbers.

Conflict of interest statement

The authors declare that there is no conflict of interest in this work.

Acknowledgements

References

[1] David Riggins, Harlan F. Nelson, Eric Johnson, Blunt-body wave drag reduction using focused energy deposition, AIAA J. 37 (4) (1999) 460–467.
[2] Viren Menezes, S. Saravanan, G. Jagadeesh, K.P.J. Reddy, Experimental investigations of hypersonic flow over highly blunted cones with aerospikes, AIAA J. 41 (10) (2003) 1955–1966.
[3] Benjamin Meyer, Harlan F. Nelson, David W. Riggins, Hypersonic drag and heat-transfer reduction using a forward-facing jet, J. Aircr. 38 (4) (2001) 680–686.
[4] Eswar Josyula, Mark Pinney, William B. Blake, Applications of a counterflow drag reduction technique in high-speed systems, J. Spacecr. Rockets 39 (4) (2002) 605–614.
[5] J.J. Marsh, L.N. Myrabo, D.G. Messitt, H.T. Nagamatsu, Yu P. Raizer, Experimental Investigation of the Hypersonic 'Air Spike' Inlet at Mach 10, AIAA Paper 96, 1996, p. 0721.
[6] D. Crawford, Investigations of the Flow over a Spiked-Nose Hemisphere-Cylinder, 1959, NASA TN D-118.
[7] Lawrence D. Huebner, Anthony M. Mitchell, Ellis J. Boudreaux, Experimental Results on the Feasibility of an Aerospike for Hypersonic Missiles, 1995, AIAA 95-0737.
[8] Ataru Sakagoshi, M. Ken, Effectiveness of an aerospike for reduction of hypersonic aerodynamic heating, in: Proceedings of 22nd International Symposium on Space Technology and Science, ISTS 2000-e-23, Morioka, Japan, 2000.
[9] Masafumi Yamauchi, Kozo Fujii, Fumio Higashino, Numerical investigation of supersonic flows around a spiked blunt body, J. Spacecr. Rockets 32 (1) (1995) 32–42.
[10] Mahmoud Ahmed, Ning Qin, Drag reduction using aerodisks for hypersonic hemispherical bodies, J. Spacecr. Rockets 47 (1) (2010) 62–80.
[11] Seymour M. Bogdonoff, Preliminary investigations of spiked bodies at hypersonic speeds, J. Aerosp. Sci. 26 (2) (1959) 65–74.
[12] C.J. Wood, Hypersonic flow over spiked cones, J. Fluid Mech. 12 (1962) 614–624.
[13] Dean R. Chapman, Donald M. Kuehn, Howard K. Larson, Investigation of Separated Flows in Supersonic and Subsonic Streams with Emphasis on the Effect of Transition, vol. 1356, ACA, 1958.
[14] G.A. Bird, Molecular Gas Dynamics and the Direct Simulation of Gas Flows, Clarendon, 1994.
[15] Arun Kumar Chinnappan, Rakesh Kumar, Modeling of high speed gas-granular flow over a 2D cylinder in the direct simulation Monte-Carlo framework, Granul. Matter 3 (18) (2016) 1–10.
[16] F.S. Donbosco, R. Kumar, Study of plume behavior of a convergent–divergent and aerospike nozzle at high altitudes using DSMC, in: Proceedings of the 29th International Symposium on Rarefied Gas Dynamics, in: AIP Conf. Proc., vol. 1628, 2014, p. 170.
[17] Claus Borgnakke, Poul S. Larsen, Statistical collision model for Monte Carlo simulation of polyatomic gas mixture, J. Comput. Phys. 18 (4) (1975) 405–420.
[18] Maxwell, J. Clerk, On stresses in rarified gases arising from inequalities of temperature, Philos. Trans. R. Soc. Lond. 170 (1879) 231–256.
[19] Jose F. Padilla, Iain D. Boyd, Assessment of gas-surface interaction models for computation of rarefied hypersonic flow, J. Thermophys. Heat Transf. 23 (1) (2009) 96–105.
[20] J.S. Wu, K.C. Tseng, C.H. Kuo, Application of local mesh refinement in the DSMC method, in: Rarefied Gas Dynamics: 22nd International Symposium, in: AIP Conf. Proc., vol. 585, 2001, pp. 417–425.
[21] Yevgeniy Bondar, Gennady Markelov, Sergey Gimelshein, Mikhail Ivanov, Numerical modeling of near-continuum flow over a wedge with real gas effects, J. Thermophys. Heat Transf. 20 (4) (2006) 699–709.
[22] Andrew J. Lofthouse, Leonardo C. Scalabrin, Iain D. Boyd, Velocity slip and temperature jump in hypersonic aerothermodynamics, J. Thermophys. Heat Transf. 22 (1) (2008) 38–49.